applied sciences

MDPI

Article

Study on Blasting Vibration Control of Brick-Concrete Structure under Subway Tunnel

Yangyong Wu [1,2], Chaomin Mu [1,2,*], Qi Zong [3], Jiehao Wu [3] and Hui Zhou [1]

[1] State Key Laboratory of Mining Response and Disaster Prevention and Control in Deep Coal Mines, Huainan 232001, China
[2] School of Safety Science and Engineering, Anhui University of Science and Technology, Huainan 232001, China
[3] School of Civil Engineering and Architecture, Anhui University of Science and Technology, Huainan 232001, China
* Correspondence: chmmu@mail.ustc.edu.cn

Abstract: In order to study the impact of the blasting vibration of subway tunnels on adjacent buildings, taking the tunnel mining method construction of the section between Zhifang Street Station and Metro Town Station of Wuhan Metro Line 27 as the engineering background, the blasting scheme is optimized by reducing the maximum single section charge, multi-section and densifying the surrounding holes. The HHT method and wavelet analysis are used to evaluate the advantages and disadvantages of the optimization scheme from the perspective of energy. The results show that the peak velocity of the blasting vibration is significantly reduced and the frequency is significantly increased after the blasting scheme is optimized. After the blasting scheme is optimized, when the working face is directly below the external wall of the building, the peak vibration velocity is the largest; from the back of the working face to the front of the working face, the peak velocity of the surface particle vibration first increases and then decreases. The frequency band of the optimized blasting vibration signal energy distribution is wider and the energy is more dispersed. This study can provide some practical experience for the design and construction of similar projects.

Keywords: subway tunnel; blasting vibration; energy distribution; Hilbert–Huang Transform model; wavelet transform

check for updates

Citation: Wu, Y.; Mu, C.; Zong, Q.; Wu, J.; Zhou, H. Study on Blasting Vibration Control of Brick-Concrete Structure under Subway Tunnel. *Appl. Sci.* **2022**, *12*, 10960. https://doi.org/10.3390/app122110960

Academic Editors: Hang Lin and Chunyang Zhang

Received: 7 October 2022
Accepted: 26 October 2022
Published: 29 October 2022

1. Introduction

With the continuous advancement of China's urbanization level, the urban population is growing rapidly, and the city size is also growing. The limited space on the ground is difficult to meet people's living needs. In order to expand people's living space, it is necessary to develop urban underground space, so as to transform urban construction from original planarization to three-dimensional [1–3]. The three-dimensional development of urban space plays a very important role in mitigating the development of cities with limited resources [4]. Development and effective use of underground space enables the city to achieve sustainable development [5,6].

At present, urban rail transit has ushered in a period of great development in China. Due to the unreasonable urban planning in China in the early stage, the subway lines are subject to many restrictions. Many subway lines have to pass through many buildings when passing through prosperous sections, and the impact on them needs to be strictly controlled when building the subway. The impact of flood and waterlogging shall be considered in design and construction [7,8]. At this stage, shield tunneling has become the mainstream method for subway construction due to its high degree of automation and fast tunnel construction speed [9–11]. However, in many cases, such as hard rock strata, there is still a place for mining law. When the subway tunnel blasting construction is carried out in an area with many buildings, the damage of the vibration generated by blasting to the buildings needs to be paid enough attention [12–14].

The research on building vibration in tunnel blasting mainly focuses on the research on peak velocity, main vibration frequency, and energy distribution of blasting vibration signals. In terms of research on vibration peak velocity, Liu et al. [15], Xia et al. [16], and Abedi et al. [17], respectively, studied the impact of blasting vibration on the vibration peak velocity of existing pipelines, concrete pipelines, and water supply pipelines; Qin et al. [18], Qian et al. [19], Zhong et al. [20], and Liu et al. [21], respectively, studied the impact of blasting vibration on the peak velocity of existing tunnel vibration based on field measurement and numerical simulation; Wang et al. [22] and Wang et al. [23] studied the impact of blasting vibration on the peak vibration velocity of 28 story frame shear wall structure and masonry structure respectively; Bayndr et al. [24] studied the influence of groundwater depth and ground tilt angle on ground vibration based on the random vibration model; Ouakka et al. [25] systematically studied the applicability and effectiveness of various measures to reduce ground vibration; Hunt et al. [26] proposed a method to calculate the vibration transmitted from railway to buildings in a two-dimensional model based on the random process theory. In terms of research on the main frequency, Meng and Guo [27] studied the characteristics of the main frequency of blasting vibration and its influencing factors by using field test methods, and obtained the prediction formula of the main frequency under specific blasting conditions; Zhou et al. [28] analyzed the attenuation mechanism and law of main frequency and average frequency of spherical charge blasting vibration through numerical simulation, and Liu et al. [29] deduced the attenuation formula of main frequency of tunnel drilling and blasting excavation blasting vibration based on dimensional analysis. In the research on the energy distribution of blasting vibration signals, mainly including the HHT method and wavelet analysis method, they are mostly used in the mining field, and the research on the impact of subway tunnel blasting vibration on surface buildings is still less. Zong et al. [30] and Qiu et al. [31] used the HHT method to study the frequency spectrum characteristics and energy distribution of blasting seismic wave signal during coal mine roadway excavation and copper mining respectively; Forrest et al. [32,33] studied the vibration response of tunnel and soil caused by vehicle load based on the Fourier-transform method, and evaluated the effectiveness of different track configurations; He et al. [34] and Zhong et al. [35] used wavelet packet energy spectrum to evaluate the impact of blasting seismic wave on building safety. At present, there are few studies on the impact of the blasting vibration of subway tunnels on surface buildings from the perspective of energy distribution.

Based on the field-measured vibration signals, this paper studies the propagation law of blasting vibration in surface buildings before and after optimization, and expands the blasting vibration signals in a time domain and frequency domain simultaneously based on the HHT method and wavelet transform, so as to evaluate the damage of subway tunnel blasting vibration to surface buildings, and avoid using the single evaluation standard of vibration peak velocity.

2. Blasting Scheme and Parameters

2.1. Project Overview

For the section from Zhifang Street Station to Metro Town Station of Wuhan Rail Transit Line 27, the subway tunnel is constructed by mining method, and the starting mileage of the section is DK44+155.54. The tunnel goes through a three-story kindergarten, which is a brick concrete structure building. The satellite map around the kindergarten is shown in Figure 1. The tunnel is designed to be 7.962 m high and 7.074 m wide. The surface environment is complex. The tunnel passes through a three-story brick concrete building. The plan is shown in Figure 2. The height from the building structure floor to the tunnel roof is 25 m.

Figure 1. Satellite map around kindergarten.

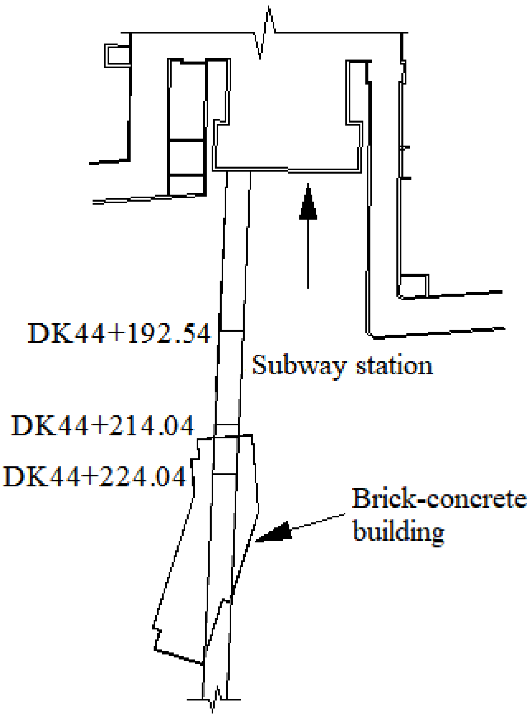

Figure 2. Plan sketch.

2.2. Blasting Scheme and Parameters

2.2.1. Blasting Scheme and Parameters before Optimization

YT–28 air-leg rock drill is used as the drilling tool. The length of the drill rod is 2.0 m and the diameter of the drill bit is 42 mm. No. 2 rock emulsion explosive is used to blast the rock in the tunnel. The diameter of the explosive roll is 32 mm, and the weight of a single explosive roll is 200 g. The millisecond delay detonators of ms 2, ms 5, ms 7, ms 9, ms 11, and other segments are used for blasting construction. The subway tunnel is full section rock, and the excavation is divided into two steps, the upper and lower steps are connected for one blasting. The upper bench shall be excavated 3–5 m in advance, and the maximum single section charge shall be 7–10 kg.

2.2.2. Blasting Scheme and Parameters after Optimization

The blasting scheme is optimized mainly through the following aspects: reducing the maximum single section charge to 3.2 kg, during millisecond blasting, increasing the segment of millisecond delay detonator, using the ms 13 segment detonator, and increasing the distance between the upper step and the lower step to reach 6–10 m.

The tunnel blasting construction adopts straight hole cutting, and the cutting hole is arranged at the lower center of the upper step, which is composed of two rounds of charging holes and empty holes in the inner ring and outer ring. The five empty holes are arranged in the center of the cutting area to increase the free surface. The depth of the cutting hole is 1.5 m, the center spacing of the empty hole is 400 mm, and the row spacing is 200 mm. The spacing of the inner ring cutting holes is 200 mm, and the spacing of the outer ring cutting holes is 400 mm. The specific cut-hole layout, detonator delay time, and network are shown in Figure 3.

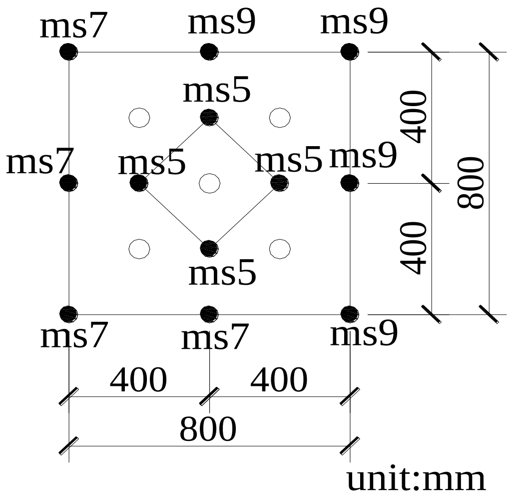

Figure 3. Manhole blasting hole layout.

Shallow hole loose blasting is adopted. The depth of the peripheral holes used as shock absorption holes is 1.6 m, and the depth of other holes is 1.2 m. The spacing between caving holes is 600 mm, the row spacing is 600 mm, and the single hole charge is 0.4 kg. The holes around the upper bench shall be detonated at last. Dense blastholes shall be arranged around the upper bench and middle bench as shock absorption holes. The distance between blastholes shall be 100mm, and the charge per hole shall be 0.1 kg. The distance between holes around the lower step is 500 mm, and the single-hole charge is 0.4 kg. The dense shock absorption holes around the upper step and middle step shall be charged in separate holes. Detonation shall be carried out in a row-by-row sequence. Each row shall be detonated with detonators of the same section. After 4–6 blasting holes in the surrounding holes and the same row of caving holes are connected in parallel, two detonators shall be used to detonate, so as to control the maximum detonating charge of a single section and ensure that the blasting vibration speed is within the specified range. The tunnel shall be blasted from top to bottom, with the row spacing of each row of blastholes being 600 mm. See Table 1 for specific blasting parameters and Figure 4 for blasthole layout.

Table 1. Blasting parameter.

Steps	Blasthole Name	Blasthole Spacing (mm)	Number of Blasthole	Blasthole Depth (m)	Charge Quantity of Single Blast-Hole (kg)	Charge Quantity (kg)	Detonator Segmentation
Upper step	Slotting holes	200, 400	12	1.5	0.8	3.2	5, 7, 9
	1st circle of caving holes	600	6	1.2	0.4	2.4	2, 9
	2nd circle of caving holes	600	11	1.2	0.4	2.4	2, 11
	Top holes	100	80	1.6	0.1	2.0	2, 15
	Bottom holes	600	11	1.2	0.4	2.4	2, 13
Middle step	Peripheral holes	100	36	1.6	0.1	0.8	5, 7, 9, 11
	1st row of caving holes	600	11	1.2	0.4	2.4	2, 5
	2nd row of caving holes	600	11	1.2	0.4	2.4	2, 7
	3d row of caving holes	600	11	1.2	0.4	2.4	2, 9
	4th row of caving holes	600	11	1.2	0.4	2.4	2, 11
Lower step	5th row of caving holes	600	9	1.2	0.4	2.4	2, 5
	6th row of caving holes	600	9	1.2	0.4	2.4	2, 7
	7th row of caving holes	600	7	1.2	0.4	2.4	2, 9
	8th row of caving holes	600	3	1.2	0.4	1.2	2, 11
	Lower peripheral holes	300, 500	25	1.2	0.4	2.4	5, 7, 9, 13

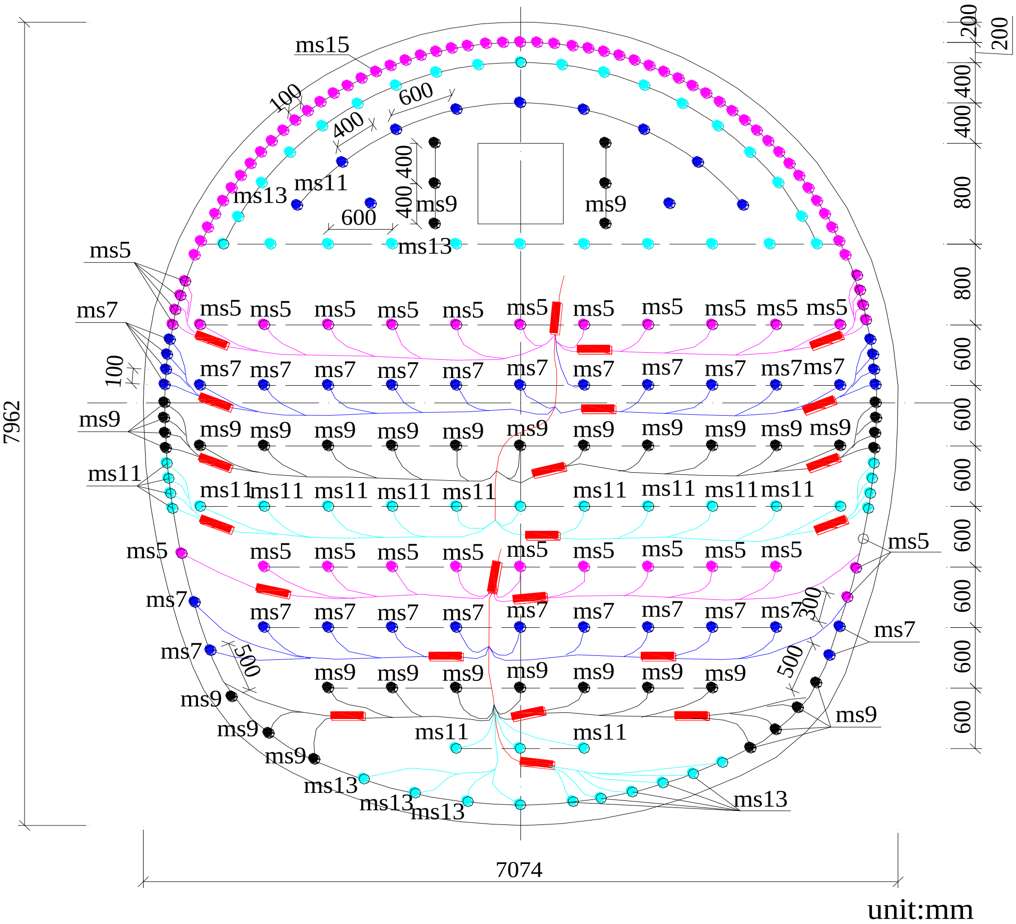

Figure 4. Blasthole layout.

2.3. Blasting Vibration Monitoring Scheme

Four NUBOX–6016 monitors are used to monitor the blasting vibration. The subway tunnel goes through a three-story kindergarten, which is a brick concrete structure building. The monitoring instruments are arranged along the footage direction to monitor the propagation law of blasting seismic wave in brick concrete structure buildings. The first of the four instruments is arranged right above the working face, the second measuring point is arranged 5 m ahead of the working face, the third measuring point is arranged 10 m ahead of the working face, and the fourth measuring point is arranged 15 m ahead of the working face. The vibration speed and frequency of the tunnel that is going through below are monitored, and the distance between the tunnel top and the ground surface is about 25 m. Figure 5 shows the layout of measuring points, and the layout of on-site measuring points is shown in Figure 6.

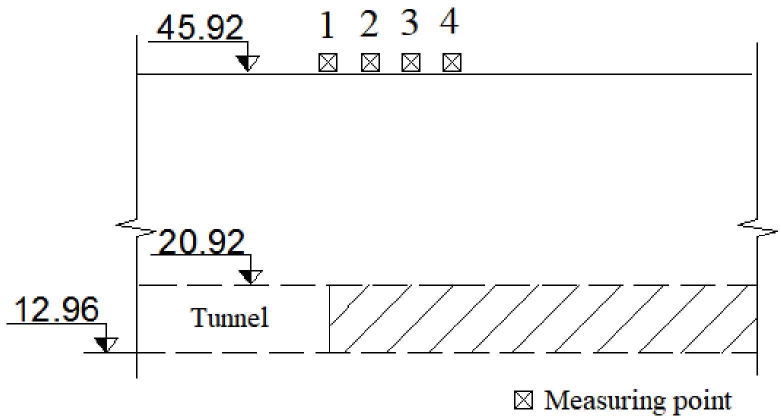

Figure 5. Survey points layout.

Figure 6. Layout of outdoor survey points.

3. Analysis of Blasting Vibration Monitoring Results

3.1. Monitoring Results

At present, blasting vibration is commonly used to use peak vibration velocity to assess structural safety [36], to carry out blasting vibration monitoring in the subway tunnel mileage section DK44+192.54~DK44+224.04, and to optimize the blasting scheme for DK44+214.044 in the subway tunnel mileage section. The monitored vibration velocity and frequency results are shown in Table 2. Groups 1 to 7 are the monitored data before the optimization of the blasting scheme, and groups 8 to 13 are the monitored data after the optimization of the blasting scheme. The typical vibration velocity time history before and after the optimization is shown in Figure 7. It can be seen from Figure 7 that the peak speed of radial vibration after scheme optimization does not decrease significantly, the peak velocity of tangential vibration decreases obviously, and the peak velocity of vertical vibration decreases significantly.

Table 2. The results of blasting vibration monitoring.

Scheme	Order Number	Vibration Peak Velocity ($cm{-}s^{-1}$)				Vibration Frequency (Hz)				Mileage of Working Face (m)	Charge Quantity (kg)
		Measuring Point 1	Measuring Point 2	Measuring Point 3	Measuring Point 4	Measuring Point 1	Measuring Point 2	Measuring Point 3	Measuring Point 4		
Before optimization	1	1.697	4.264	1.904	0.95	1.53	1.53	1.53	1.53	DK44+192.54	9
	2	1.431	2.512	1.417	0.806	1.53	1.53	1.53	1.53	DK44+195.04	7
	3	2.532	3.228	3.21	0.764	3.66	1.53	1.53	1.83	DK44+197.04	8
	4	2.255	4.302	1.997	1.81	1.53	1.53	1.53	1.53	DK44+199.04	10
	5	3.203	4.603	1.106	0.921	2.44	2.75	3.66	3.66	DK44+205.04	10
	6	3.842	3.852	1.408	1.115	2.14	2.14	1.53	1.53	DK44+206.54	10
	7	1.861	2.251	1.532	1.043	3.36	3.36	3.36	3.36	DK44+208.54	10
After optimization	8	1.096	1.567	1.347	0.873	1.83	2.14	2.14	6.1	DK44+214.04	3.2
	9	1.109	1.27	1.093	0.856	1.53	3.36	1.53	1.53	DK44+215.54	3.2
	10	1.183	1.244	1.303	0.885	2.44	3.97	3.66	2.44	DK44+217.04	3.2
	11	1.277	1.835	1.533	0.926	1.83	1.83	1.83	1.83	DK44+219.04	3.2
	12	0.607	1.398	0.818	0.636	2.14	2.14	4.27	2.14	DK44+222.04	3.2
	13	0.994	0.969	0.78	0.693	6.1	6.41	6.41	6.41	DK44+224.04	3.2

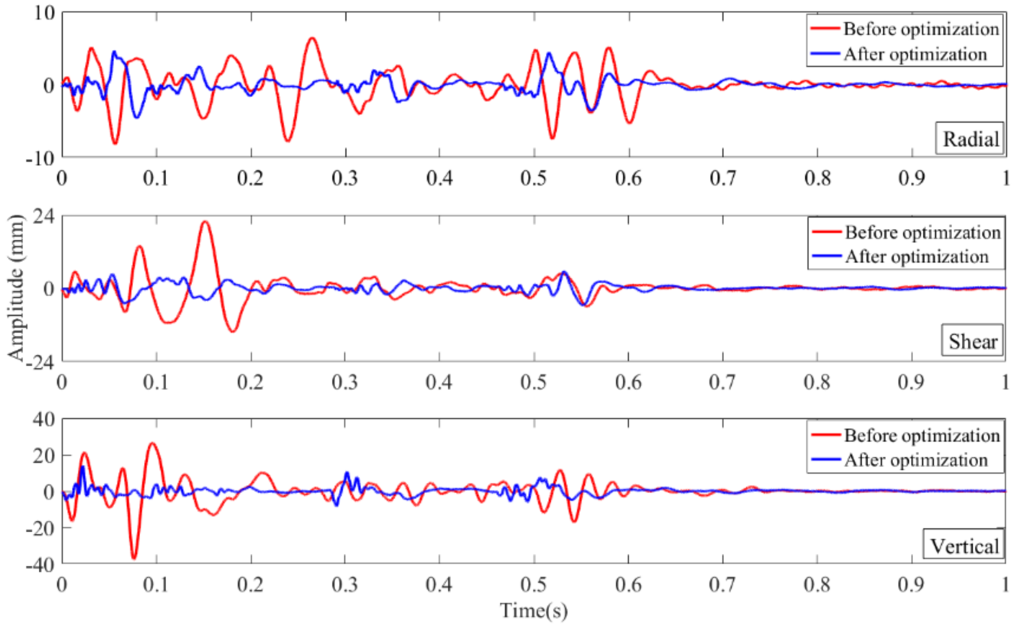

Figure 7. The typical blasting vibration time-distance graph before and after optimization.

3.2. Propagation Law of Blasting Vibration

According to the stipulations in the blasting safety regulations GB6722–2014 [37], due to the low vibration frequency of brick concrete structure buildings, the allowable safe vibration velocity is 1.5–2.0 cm/s. Before the optimization of the blasting scheme, the measured peak vibration velocity is in the range of 0.764–4.603 cm/s. After the blasting scheme is optimized, the measured vibration peak velocity is within the range of 0.607–1.835 cm/s, which is less than 2.0 cm/s. The vibration peak velocity after the blasting scheme is optimized meets the safety requirements specified in the blasting safety regulations.

According to Table 2, the relationship between the vibration peak speed and the position of the working face is drawn, as shown in Figure 8.

In the forward direction of the subway tunnel work, the peak vibration velocity before the optimization of the blasting scheme is significantly greater than the peak vibration velocity after the optimization of the blasting scheme, which shows that the effect of the optimization of the blasting scheme is very significant.

After the optimization of the blasting scheme, the peak vibration speed is relatively high when the working face mileage is DK44+219.04. This is the exterior wall of the brick concrete structure kindergarten. When the working face mileage is greater than DK44+219.04, it enters the kindergarten. When the working face mileage is less than DK44+219.04, it enters the road surface. When blasting seismic wave propagates in rock and soil, the denser the rock and soil, the higher the wave velocity, the looser the rock and soil, the lower the wave velocity [38]. During the blasting operation in the subway tunnel, the blasting seismic wave propagates from the blasting source to the buildings on the ground. Because the materials at the foundation are relatively dense, the wave velocity of the blasting seismic wave propagating to the buildings through the foundation will be higher, and the blasting vibration effect caused by it will be greater. When the working face mileage is DK44+219.04, the foundation is below, and the bearing wall is above the foundation. The density of materials is very good, which is far greater than the density on both sides of the wall. When the blasting seismic wave propagates upward from the blasting source, because the density of the working face mileage at DK44+219.04 is greater than that on both sides, according to the theory mentioned above, the wave speed transmitted here during blasting is greater than that on both sides, and the vibration speed of the ground surface is also greater than that on both sides.

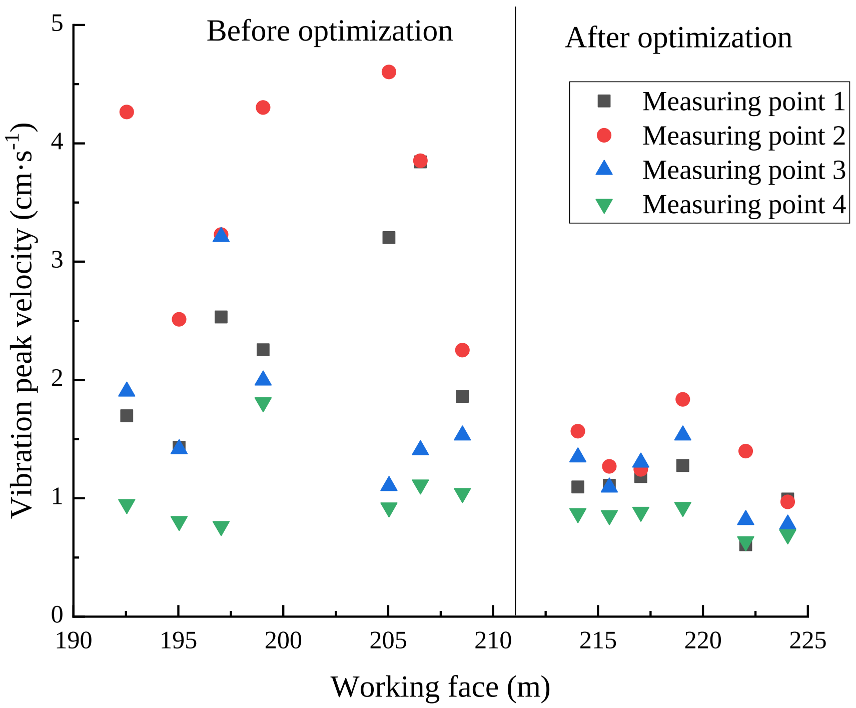

Figure 8. The situation of the blasting vibration velocity changing with working face location.

According to the data in Table 2, the relationship between the vibration peak speed and the location of the measuring point is drawn, as shown in Figure 9. Digital Group1-13 in the figure represents 13 field tests.

According to Figure 9, for the monitored measuring points, the peak vibration velocity increases first and then decreases from near to far from the working face, and the peak vibration velocity of the surface particle is the largest at 5 m in front of the working face.

The reasons for this conclusion can be explained by the following two points. First is the void effect. The peak velocity of surface particle vibration increases from the surface particle above the working face to 5 m in front of the working face because the working face is free and part of the energy will be lost to the air during blasting. The decrease in the peak velocity of vibration when passing 5 m in front of the working face is due to the growth of the propagation path and the attenuation of the energy. Yu et al. [39] and Shi et al. [40] studied the blasting vibration cavity effect using the method based on experiment and numerical simulation and obtained so that the vibration velocity amplification coefficient first increased and then decreased with the increase of the horizontal distance from the blasting source. The second is the diffraction of stress waves [41]. The reflection and superposition of the stress wave between the surface and the upper surface of the channel is obvious, which makes the attenuation of the peak velocity of the surface particle vibration slow. The peak vibration velocity at the second measuring point reached the maximum, and the particle vibration velocity on the ground in front of the working face showed a trend of first increasing and then decreasing.

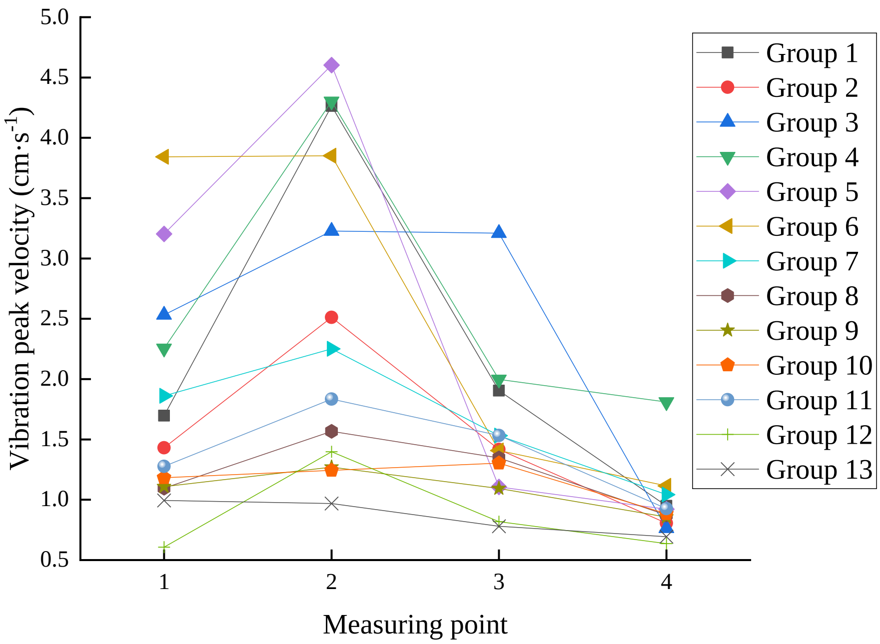

Figure 9. The situation of the blasting vibration velocity changes with measuring point location.

3.3. Distribution Law of Blasting Vibration Frequency

According to the data in Table 2, the law of blasting vibration frequency changing with the position of the working face is drawn, as shown in Figure 10.

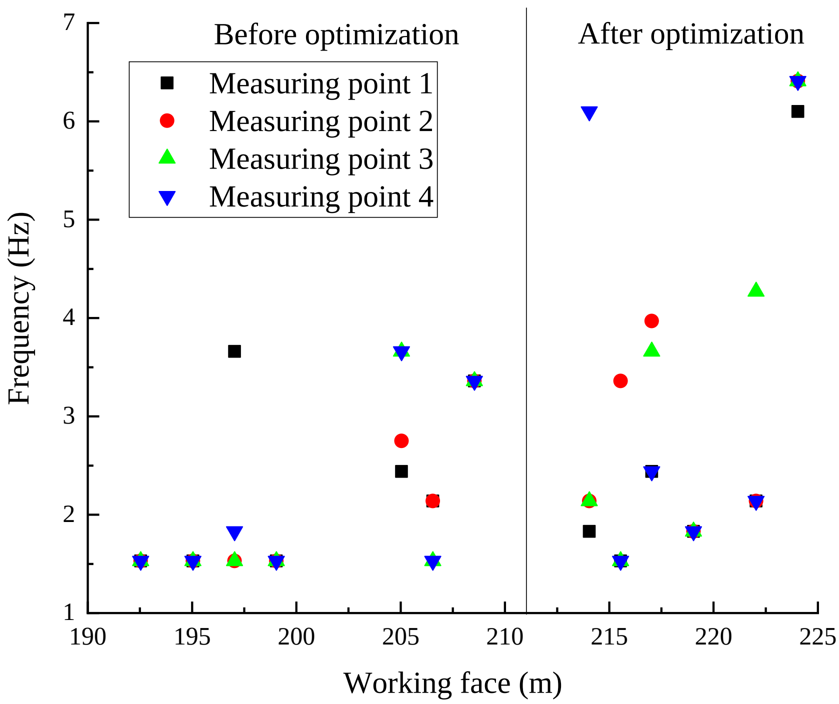

Figure 10. The situation of the frequency changing with working face location.

Before the optimization of the blasting scheme, during the blasting construction, the working face mileage is located at DK44+192.54.200–DK44+214.04, and the maximum single section charge is 7–10 kg. During the blasting construction, 7 sets of data were monitored, 28 blasting vibration signals were measured, and the blasting vibration frequency measured at the measuring point was within the range of 1.53–3.66 Hz. After the optimization of the blasting scheme, during the blasting construction, the working face mileage is located at DK44+214.04–DK44+224.04, and the maximum single section charge is 2.4–3.2 kg. During the blasting construction, six times of monitoring were conducted and six groups of measured data were obtained, with a total of 24 blasting vibration signals. The measuring points were arranged in the brick concrete structure building, and the measured blasting vibration frequency was 1.53–6.41 Hz, mainly concentrated in 1.53–5.00 Hz. By comparing the monitored blasting vibration frequencies before and after the optimization of the blasting scheme in Table 2 and the distribution of blasting vibration before and after the optimization of the blasting scheme in Figure 8, the optimization of the blasting scheme can be obtained, which significantly increases the blasting vibration frequency. The reference [37] stipulates that the allowable safety standards for blasting vibration in China consider both blasting vibration frequency and blasting vibration speed. For the same object, when the blasting vibration frequency is low, the safety allowable vibration speed is small. Since the natural vibration frequency of the brick concrete structure building is low, the blasting vibration frequency of the brick concrete structure building after the blasting scheme optimization becomes larger, which makes it more difficult to form resonance phenomenon, and the building is safer.

4. Spectrum and Energy Analysis of Blasting Vibration Signal

4.1. Signal Decomposition and Analysis

4.1.1. EMD Decomposition and Analysis of Signals

The original signals measured in the field before and after the scheme optimization are relatively complex, so it is very difficult to analyze them directly. The primary task to obtain the signal is to decompose it, and then analyze the components obtained after decomposition. The EMD method does not require preset basis functions and has the advantages of adaptability and efficiency [42]. The original signals can be decomposed into components by the EMD method. These components are different in time scale, and these IMF components contain the original signal's own characteristics. These IMF components have specific and practical physical meanings, and they can express the most outstanding information of the original signal.

The blasting vibration signal is decomposed by EMD in multiple layers, and IMF components and power spectral density (PSD) will be obtained from the decomposition. They are shown in Figure 11. Figure 11a shows the IMF component of the original signal before scheme optimization, Figure 11b shows the power spectral density (PSD) of the original signal before scheme optimization, Figure 11c shows the IMF component of the original signal after scheme optimization, and Figure 11d shows the power spectral density (PSD) of the original signal after scheme optimization.

It can be seen from Figure 11a,b that twelve components of c1–c11 and R are obtained after EMD decomposition of the signal before scheme optimization. The amplitude and frequency of different IMF components are different. Most of the IMF components obtained by EMD are of physical significance; c1 represents the white noise contained in the signal, and c2 and c3 represent the high frequency of the signal. The most important part of the vibration signal is composed of c4–c6. Their vibration amplitude is relatively large. The dominant range of the frequency corresponding to c4 is 20–40 Hz, the dominant range of the frequency corresponding to c5 is 40–50 Hz, and the dominant range of the frequency corresponding to c6 is 0–20 Hz. The secondary part of the signal is composed of components c7–c11 with small amplitude and frequency of vibration velocity, whose frequency is within 20 Hz, and component R is the residual quantity of blasting vibration signal.

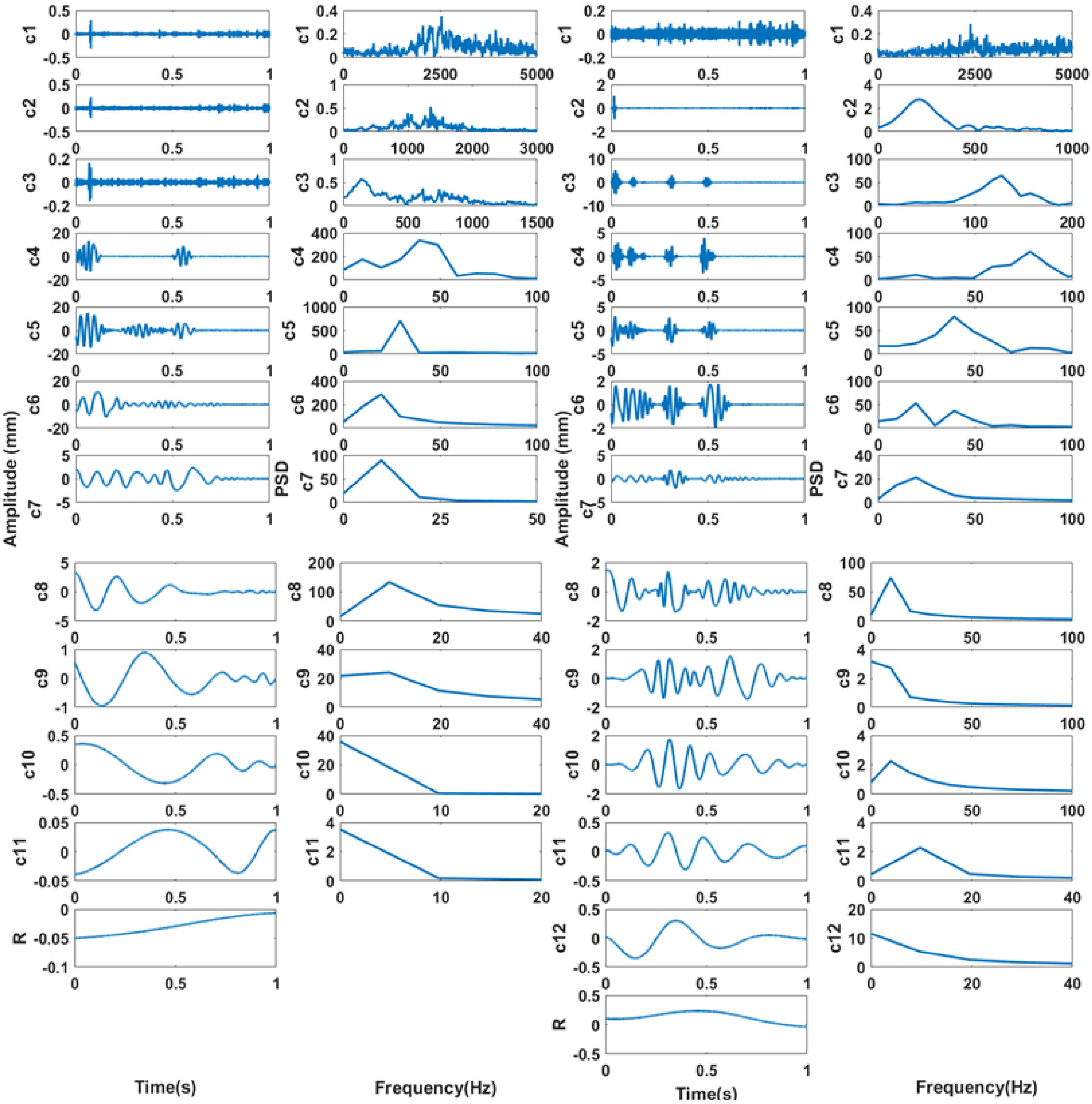

(**a**) (**b**) (**c**) (**d**)

Figure 11. The result of EMD resolution before and after optimization (**a**) the IMF component of the original signal before scheme optimization (**b**) the power spectral density (PSD) of the original signal before scheme optimization (**c**) the IMF component of the original signal after scheme optimization and (**d**) the power spectral density (PSD) of the original signal after scheme optimization.

It can be seen from Figure 11c,d that thirteen components of c1–c12 and R are obtained after EMD decomposition of the optimized signal; c1 is the white noise contained in the signal, and c2 is the high-frequency component of the signal. The most important part of the vibration signal is composed of c3–c7. Their vibration amplitude is relatively large. The dominant range of the frequency corresponding to c3 is 100–150 Hz, the dominant range of the frequency corresponding to c4 is 50–100 Hz, the dominant range of the frequency corresponding to c5 is 20–50 Hz, the dominant range of the frequency corresponding to c6 is 0–50 Hz, and the dominant range of the frequency corresponding to c7 is 0–50 Hz. The secondary part of the signal is composed of components c8–c12 with small amplitude and frequency of vibration velocity, whose frequency is within 30Hz, and component R is the residual quantity of blasting vibration signal.

The EMD method is used to decompose the original signal, and the IMF component is obtained. The IMF component contains white noise and high-frequency of the signal with a small amount of energy. The white noise and high frequency should be filtered out to avoid their interference, so as to obtain a higher signal-to-noise ratio and more useful information. Low pass filtering is used to filter out the white noise and high frequency of the signal, leaving the required IMF component and reconstructing it to obtain the filtered signal. After the interference signal is eliminated, the signal analysis can be more accurate and effective.

By comparing Figure 11a,c, it can be concluded that the maximum amplitude of IMF component vibration before the scheme optimization is about 20mm, and the maximum amplitude of IMF component vibration after the scheme optimization is about 10mm, which is very significant. By comparing Figure 11b,d, it can be concluded that the dominant range of the frequency before the optimization of the scheme is 0–50 Hz, and the dominant range of the frequency after the optimization of the scheme is 0–150 Hz, and the dominant frequency increases significantly; the maximum power spectral density before scheme optimization is about 1000 W/Hz, and the maximum power spectral density after scheme optimization is about 100 W/Hz. The power spectral density decreases significantly. For this building, the greater the blasting frequency is, the safer it will be. After the scheme is optimized, the blasting construction process will be safer.

4.1.2. Wavelet Decomposition and Analysis of Signals

The wavelet transform needs to select the wavelet base first, and then transform. The signal reconstruction and error of the original signal based on the db3, db5, db8, and coif3 wavelet bases are very close to the original signal after reconstruction based on the four wavelet bases, but the reconstruction error of the original signal based on the db8 wavelet base is the smallest, about 2×10^{-11} mm, so db8 is selected as the wavelet basis for wavelet decomposition of the original signal.

Figure 12 shows the wavelet decomposition of the original signal before and after the blasting scheme optimization. Figure 12a shows the wavelet decomposition of the original signal before blasting scheme optimization, and Figure 12b shows the wavelet decomposition of the original signal after blasting scheme optimization. D1–D8 and A8 in Figure 12a,b are wavelet components, where the high-frequency components are D1–D8 and the low-frequency components are A8. It can be seen from Figure 12 that the maximum component of the wavelet component before the blasting scheme optimization is greater than the maximum component of the wavelet component before the blasting scheme optimization, which also proves that the blasting construction effect after the blasting scheme optimization is better than before.

4.2. Spectrum and Energy Analysis

4.2.1. Energy Analysis Based on HHT Method

Before and after the optimization of the blasting scheme, the frequency and PSD distribution of monitored blasting vibration signals are shown in Figure 13. It can be seen from Figure 13 that the low-frequency range is the place where the signal energy is most concentrated before optimization, and this range is below 100 Hz. The energy is evenly distributed in the range of 60–100 Hz frequency band. The energy is obviously increased in the range of 0–60 Hz frequency band, and the energy is maximum in the range of 20–40 Hz frequency band, and a maximum value is shown. Compared with the PSD diagram shown in Figure 11b, the dominant range of the frequency corresponding to c3 is 20–40 Hz, and the amplitude is also the largest. The dominant range of frequencies corresponds to c4 and c5 is 40–50 Hz and 0–20 Hz, and there is also a relatively large amplitude.

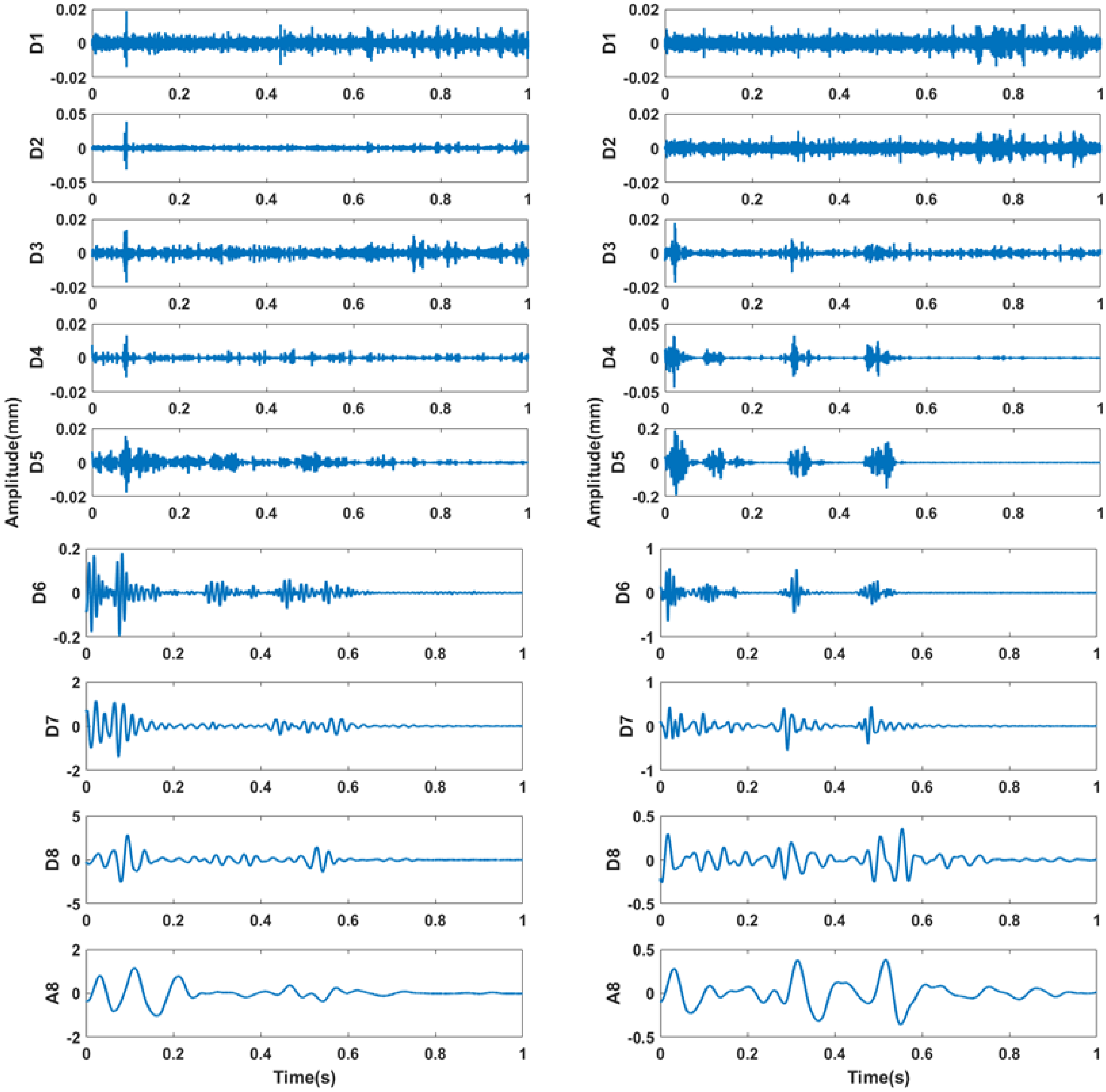

(a) (b)

Figure 12. The result of Wavelet resolution (**a**) before optimization and (**b**) after optimization.

The low-frequency range is also the place where the signal energy is most concentrated after optimization, which is below 300 Hz. The energy is evenly distributed in the range of 150–250 Hz frequency band. When the energy is obviously increased in the range of the 0–150 Hz frequency band, and the energy is at maximum in the range of the 0–20 Hz frequency band, a maximum value appears. Compared with the PSD diagram shown in Figure 11d, the dominant range of the frequency corresponding to c1 is 100–150 Hz, and the amplitude is also the largest. The dominant range of frequencies corresponding to components c2, c3, c4, and c5 is 50–100 Hz, 20–50 Hz, 0–50 Hz, and 0–50 Hz, they also have relatively large amplitudes.

The relationship between the amplitude and time of the energy contained in the blasting vibration signal monitored before and after optimization is shown in Figure 14. It can be seen from Figure 14 that the energy of signal vibration before optimization is mainly concentrated in three periods: 0 s–0.16 s, 0.19 s–0.50 s, 0.51 s–0.58 s. It can be seen from the time history chart of vibration speed in Figure 7 that the change of instantaneous energy in time is consistent with the change of energy contained in the monitored vibration signal in size. The order of occurrence of the larger points in the peak value is 0.08 s, 0.21 s, 0.49 s, 0.53 s.

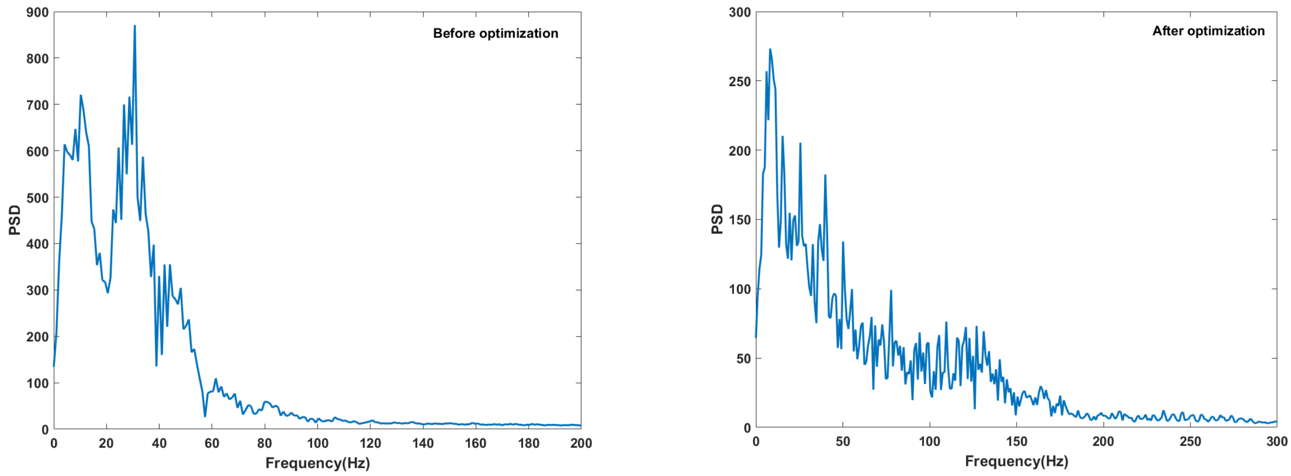

(**a**) (**b**)

Figure 13. The spectrum of blasting vibration signal (**a**) before optimization and (**b**) after optimization.

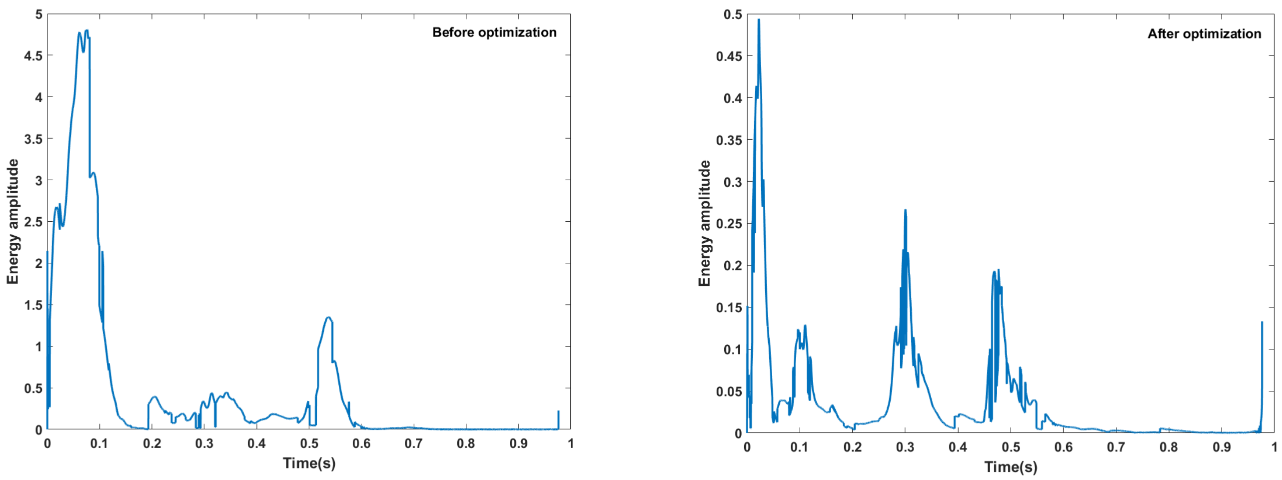

(**a**) (**b**)

Figure 14. The energy amplitude of blasting vibration signal (**a**) before optimization and (**b**) after optimization.

The vibration energy is mainly concentrated in three periods: 0 s–0.19 s, 0.20 s–0.40 s, and 0.41 s–0.55 s. It can be seen from the time history chart of vibration speed in Figure 7 that the change of instantaneous energy in time is consistent with the change of energy contained in the monitored vibration signal in size. The order of occurrence of the larger points in the peak value is 0.03 s, 0.11 s, 0.30 s, 0.48 s.

Before and after the optimization of the blasting scheme, the Hilbert energy spectrum of the monitored blasting vibration signal is shown in Figures 15 and 16. It reflects the relationships between time, frequency, and instantaneous energy. Different colors in Figure 15 indicate different energies. The redder the color, the greater the energy. For the signal before optimization, when the time sampling point is in the range of 100–1800 and the frequency is in the range of 0–30 Hz, there are many red points gathered in the range, indicating that the vibration energy is mainly concentrated in this area. Divide the time sampling point by the sampling frequency to calculate the time of energy concentration as 0.01 s–0.18 s, which is basically consistent with the time period in Figure 14. For the optimized signal, when the time sampling point is in the range of 200–1100 and the frequency is in the range of 0–50 Hz, there are many red points gathered in the range, indicating that the vibration energy is mainly concentrated in this area. Divide the time sampling point by the sampling frequency to calculate the time of energy concentration as 0.02 s–0.11 s, which is basically consistent with the time period in Figure 14. The three-dimensional energy spectrum can be obtained by applying the Hilbert transform, as shown in Figure 16. When frequency and time change, the distribution of energy also changes, which can be seen more directly from Figure 16.

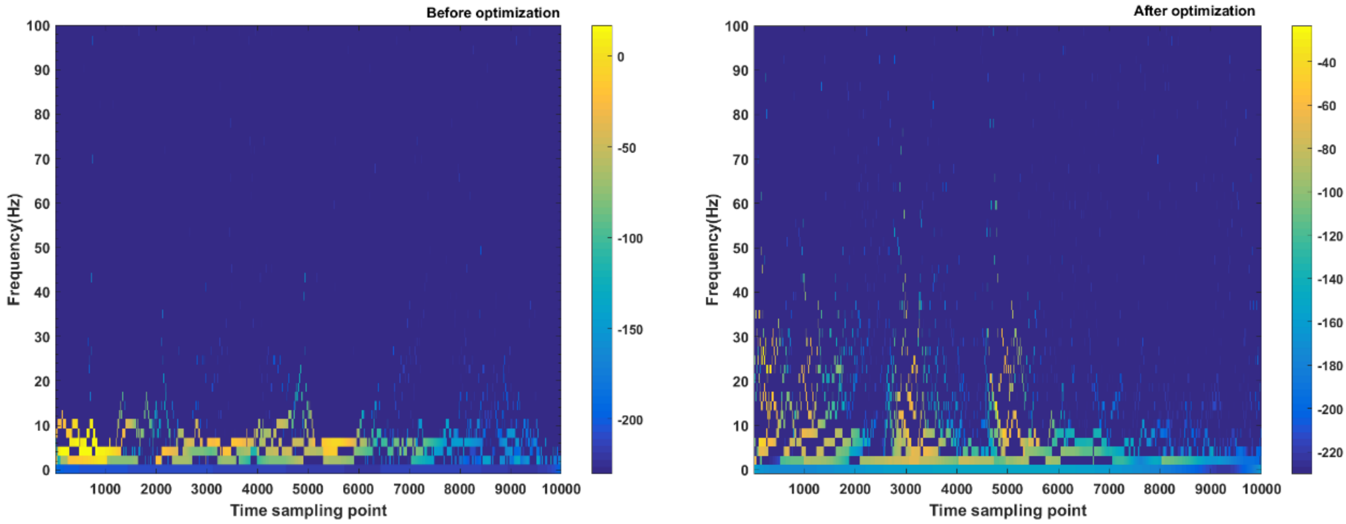

(a) (b)

Figure 15. The Hilbert energy spectrum of blasting vibration signal (**a**) before optimization and after (**b**) optimization.

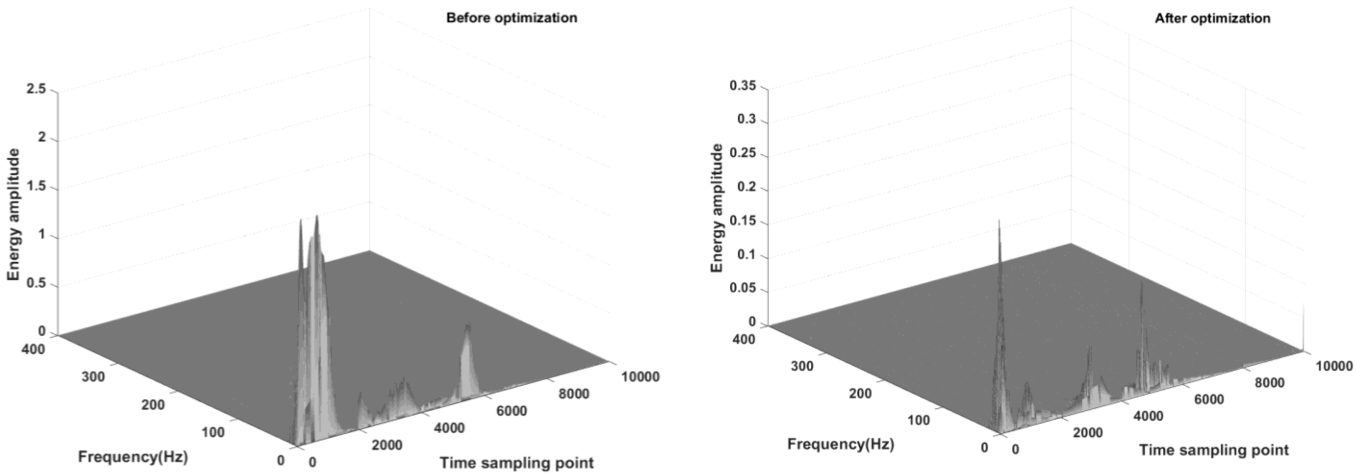

(a) (b)

Figure 16. The Hilbert's three-dimensional energy spectrum of blasting vibration signal (**a**) before optimization and (**b**) after optimization.

4.2.2. Energy Analysis Based on Wavelet Transform

Firstly, db8 is selected as the wavelet base. Then, the blasting vibration signals before and after blasting scheme optimization are transformed by the wavelet transform. Finally, the frequency band energy distribution diagram of the blasting vibration signal is obtained, as shown in Figure 17.

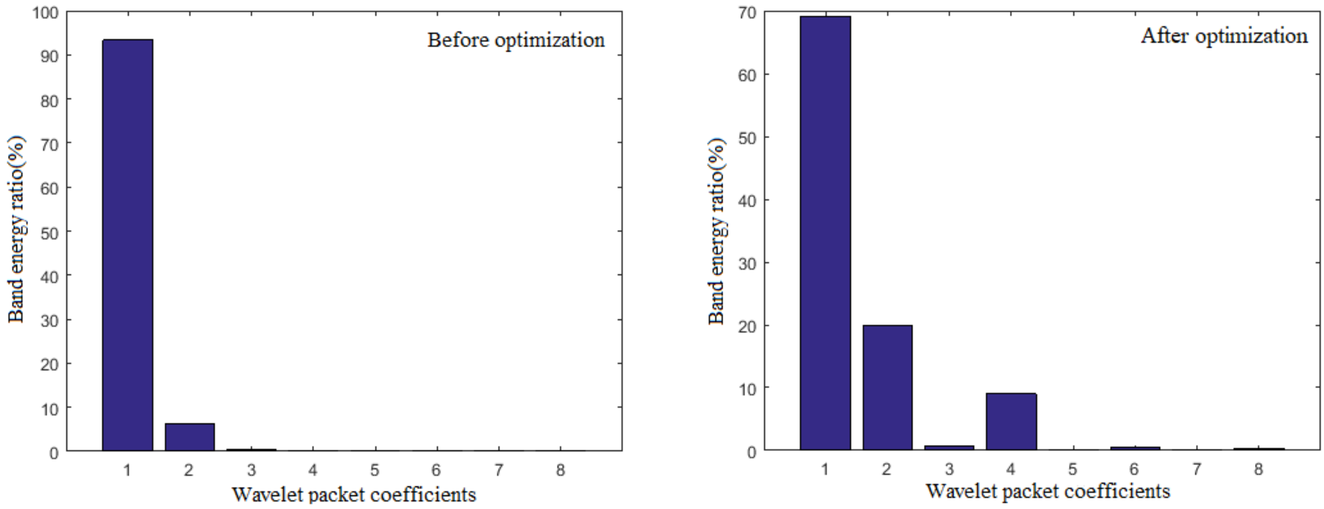

(**a**) (**b**)

Figure 17. Band energy distribution diagram of blasting vibration signal (**a**) before optimization and (**b**) after optimization.

For the signal before optimization, only the first three frequency bands have energy. The energy in the first frequency band accounts for about 95% of the total energy, the energy in the second frequency band accounts for about 5% of the total energy, and the energy in the third frequency band is negligible. The energy contained in the monitored blasting vibration signal before the optimization of the blasting scheme is mainly concentrated in the 0–62.5 Hz frequency band; For the optimized signal, there is energy in the 1st, 2nd, 3rd, 4th, 6th, and 8th frequency bands, of which the energy in the 1st frequency band accounts for about 70% of the total energy, the energy in the 2nd frequency band accounts for about 20% of the total energy, the energy in the 4th frequency band accounts for about 10% of the total energy, and the energy in the 3rd, 6th, and 8th frequency bands is relatively small, which can be ignored. The energy contained in the blasting vibration signal monitored before the blasting scheme optimization is mainly concentrated in the 0–125 Hz frequency band. It can be seen from Figure 17 that after the optimization of the blasting scheme, the energy contained in the blasting vibration signal is more widely distributed in the frequency band and less distributed in the low frequency. The less energy distributed in the low frequency is more conducive to the safety of brick concrete structure buildings, which shows that the optimized scheme has achieved a good blasting construction effect.

The blasting vibration signals before and after the blasting scheme optimization are wavelet transformed to obtain the three-dimensional energy spectrum of the blasting vibration signal. The yellow part indicates the higher relative energy, as shown in Figure 18. The maximum relative energy amplitude before the optimization is about 4, and the maximum relative energy amplitude after optimization is about 0.6. Compared with the Hilbert three-dimensional energy spectrum of blasting vibration signals before and after optimization in Figure 16, the maximum relative energy amplitude is about 5 and 0.5, respectively. The difference between the two results is small, and the results are in good agreement.

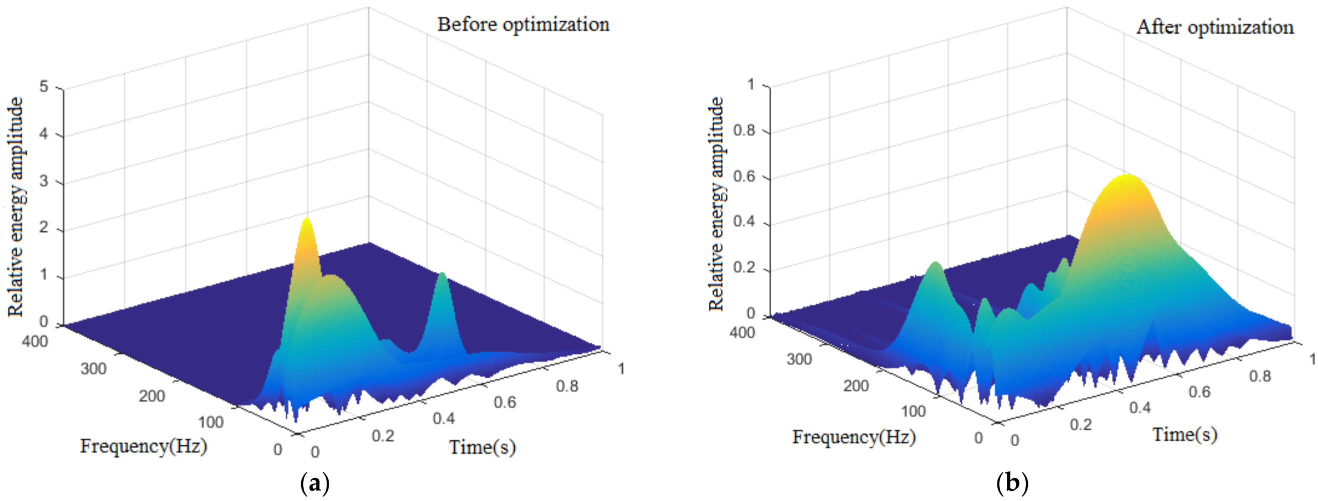

Figure 18. The three-dimensional energy spectrum of blasting vibration signal (**a**) before optimization and (**b**) after optimization.

5. Conclusions

This paper is based on the underground excavation of the tunnel between Zhifang Street Station and Metro Town Station of Wuhan Metro Line 27. In order to make the subway tunnel pass through the brick concrete structure buildings safely, the blasting scheme is optimized by reducing the maximum single-section and multi-section charges, increasing the distance between the upper and lower steps, and densifying the surrounding holes. Based on the field experiment results, the HHT method and wavelet analysis are used to evaluate the advantages and disadvantages of the optimization scheme from the perspective of energy. The HHT method first decomposes the signal by EMD, then obtains the MF component and power spectral density (PSD), and finally, the distribution of frequency and PSD, the relationship between energy amplitude and time, and the Hilbert energy spectrum of vibration signal are further obtained. In the wavelet transform, db8 is selected as the wavelet base, then the wavelet components are obtained through transformation, and finally, the frequency band energy distribution and three-dimensional energy spectrum are obtained. The following conclusions are obtained:

1. The peak velocity and frequency of vibration at monitoring points before and after the optimization of blasting schemes were monitored. The peak velocity of blasting vibration after the optimization of the blasting scheme was significantly lower than that after the optimization of the blasting scheme, and both were less than 2.0 cm/s; The blasting vibration frequency after the optimization of the blasting scheme is significantly higher than that before the optimization of the blasting scheme, which is more difficult to form resonance, and the building is safer.
2. After the blasting scheme is optimized, the peak vibration velocity is at maximum when the blasting construction is directly under the exterior wall of the brick concrete structure. When blasting to such parts, the maximum single-section charge shall be kept as small as possible, and millisecond blasting shall be used for multi-section blasting.
3. Within the monitoring range, from the back of the working face to the front of the working face, the peak velocity of surface particle vibration increases first and then decreases. The peak velocity of surface particle vibration is the largest at 5 m in front of the working face, and the cavity effect and diffraction of the stress wave are obvious.
4. From the perspective of energy, the optimized blasting scheme has a wider frequency band of measured vibration signal energy distribution, a more decentralized energy, and a safer optimized scheme than before.

Author Contributions: Conceptualization, Q.Z. and J.W.; methodology, Y.W.; software, Y.W.; validation, Y.W., C.M., and Q.Z.; formal analysis, Y.W.; investigation, H.Z.; resources, Q.Z.; data curation, Y.W.; writing—original draft preparation, Y.W.; writing—review and editing, Y.W.; visualization, Y.W.; supervision, C.M.; project administration, Q.Z.; funding acquisition, Q.Z. All authors have read and agreed to the published version of the manuscript.

Funding: This research was funded by the National Natural Science Foundation of China, grant number 51404010.

Institutional Review Board Statement: Not applicable.

Informed Consent Statement: Not applicable.

Data Availability Statement: The data used to support the findings of this study are available from the corresponding author upon request.

Conflicts of Interest: The authors declare no conflict of interest.

References

1. Hao, M.; Wang, D.; Deng, C.; He, Z.; Zhang, J. 3D geological modeling and visualization of above-ground and underground integration-taking the Unicorn Island in Tianfu new area as an example. *Earth Sci. Inform.* **2019**, *12*, 465–474. [CrossRef]
2. Xi, Y.; Li, X.; Zhu, H.; Zhang, W.; Zhao, S.; Xu, W. Three-dimensional high-precision assessment of mountainous urban underground space resources: A case study in Chongqing, China. *Tunn. Undergr. Space Technol.* **2022**, *123*, 104439. [CrossRef]
3. Wang, Y.; Yue, X.; Li, C.; Wang, M.; Zhang, H.; Su, Y. Relationship between urban three-dimensional spatial structure and population distribution: A case study of Kunming's main urban district, China. *Remote Sens.* **2022**, *14*, 3757. [CrossRef]
4. Shao, F.; Shi, P.; Ding, Y.; Dong, C. The integrated development strategy of coastal Industrial areas and city based on underground space development. *Geofluids* **2021**, *2021*, 4336163. [CrossRef]
5. Zhang, Y.; Zhu, J.; Liao, Z.; Guo, J.; Peng, Q. An intelligent planning model for the development and utilization of urban underground space with an application to the Luohu District in Shenzhen. *Tunn. Undergr. Space Technol.* **2021**, *112*, 103933. [CrossRef]
6. Wang, Z. Land spatial development based on carrying capacity, land development potential, and efficiency of urban agglomerations in China. *Sustainability* **2018**, *10*, 4701. [CrossRef]
7. Lin, Z.; Hu, S.; Zhou, T.; Zhong, Y.; Zhu, Y.; Shi, L.; Lin, H. Numerical simulation of flood intrusion process under malfunction of flood Retaining facilities in complex subway stations. *Buildings* **2022**, *12*, 853. [CrossRef]
8. Liu, B.; Lin, H.; Chen, Y.; Liu, J.; Guo, C. Deformation stability response of adjacent subway tunnels. *Lithosphere* **2022**, *2022*, 7227330. [CrossRef]
9. Zhang, C.; Zhao, Y.; Zhang, Z.; Zhu, B. Case study of underground shield tunnels in interchange piles foundation underpinning construction. *Appl. Sci.* **2021**, *11*, 1611. [CrossRef]
10. Fang, Q.; Du, J.; Li, J.; Zhang, D.; Cao, L. Settlement characteristics of large-diameter shield excavation below existing subway in close vicinity. *J. Cent. South Univ.* **2021**, *28*, 882–897. [CrossRef]
11. Wang, C. Influence of underground geotechnical operation on surface buildings through the shield method. *Arab. J. Geosci.* **2019**, *12*, 1–6. [CrossRef]
12. Zhao, H.; Long, Y.; Li, X.; Lu, L. Experimental and numerical investigation of the effect of blast-induced vibration from adjacent tunnel on existing tunnel. *KSCE J. Civ. Eng.* **2016**, *20*, 431–439. [CrossRef]
13. Jiang, N.; Zou, R.; Qu, Y.; Xu, Q.; Li, Z. Numerical analysis of the subway tunnel vibration monitoring near the blasting excavation. *Eng. Blasting* **2013**, *19*, 46–49+45.
14. Li, S.; Li, K.; Lei, G.; Sun, G. Study of blasting vibration and deformation control for metro construction beneath existing metro tunnel in short distance. *Rock Soil Mech.* **2014**, *35*, 284–289.
15. Liu, X.; Jiang, A.; Guo, X.; Hai, J. Effect of excavation blasting in the arch cover method on adjacent existing pipelines in a subway station. *Appl. Sci.* **2022**, *12*, 1529. [CrossRef]
16. Zhang, Z.; Zhou, C.; Lu, S.; Jiang, N.; Wu, C. Dynamic response characteristic of adjacent buried concrete pipeline subjected to blasting vibration. *J. Harbin Inst. Technol.* **2017**, *49*, 79–84.
17. Xia, Y.; Jiang, N.; Zhou, C.; Luo, X. Safety assessment of upper water pipeline under the blasting vibration induced by Subway tunnel excavation. *Eng. Fail. Anal.* **2019**, *104*, 626–642. [CrossRef]
18. Qin, Q.; Zhang, J. Vibration control of blasting excavation of large cross-section highway tunnel over metro line. *Arab. J. Geosci.* **2020**, *13*, 868. [CrossRef]
19. Qian, Y.; Wang, X. Study on safety influence of blasting construction close to existing tunnel. *Beijing Jiaotong Univ.* **2014**, *38*, 90–96.
20. Zhong, D.; Wu, L.; Yu, G. Effect of tunneling blasting on an existing adjacent tunnel. *Explos. Shock Waves* **2010**, *30*, 456–462.
21. Liu, D.; Song, G.; Chu, F.; Cheng, J.; Zeng, J. Numerical analysis of the effects of the tunnel blasting on the nearby tunneling areas. *J. Saf. Environ.* **2014**, *14*, 64–68.

22. Wang, L.; Gao, W.; Zhang, F.; Cao, X. Research on blasting vibration response of high-rise building based on model simplification. *Acta Armamentarii* **2018**, *39*, 121–134.
23. Wang, X.; Guan, X.; Yu, Y.; Li, W. Local dynamic stress response and damage of structure under tunnel blasting vibration. *Chin. J. Undergr. Space Eng.* **2019**, *15*, 125–133.
24. Bayndr, C. Effects of ground water table and ground inclination on train induced ground-borne vibrations. *TWMS J. Appl. Eng. Math.* **2019**, *9*, 735–746.
25. Ouakka, S.; Verlinden, O.; Kouroussis, G. Railway ground vibration and mitigation measures: Benchmarking of best practices. *Railw. Eng. Sci.* **2022**, *30*, 1–22. [CrossRef]
26. Hunt, H. Modelling of rail vehicles and track for calculation of ground-vibration transmission into buildings. *J. Sound Vib.* **1996**, *193*, 185–194. [CrossRef]
27. Meng, H.; Guo, F. Experimental research on the master frequency of blasting seismic wave. *J. Railw. Eng. Soc.* **2009**, *11*, 81–83.
28. Zhou, J.; Lu, W.; Zhang, L.; Chen, M.; Yan, P. Attenuation of vibration frequency during propagation of blasting seismic wave. *Chin. J. Rock Mech. Eng.* **2014**, *33*, 2171–2178.
29. Liu, D.; Lu, W.; Chen, M.; Yan, P. Attenuation formula of the dominant frequency of blasting vibration during tunnel excavation. *Chin. J. Rock Mech. Eng.* **2018**, *37*, 2015–2026.
30. Zong, Q.; Wang, H.; Xu, Y.; Fu, J. Analysis of blasting seismic wave signal in coalmine roadway excavation based on HHT method. *J. Vib. Shock* **2013**, *32*, 116–120.
31. Qiu, X.; Shi, X.; Zhou, J.; Dan, H.; Xin, C. On vibration reduction effect of short millisecond blasting by high-precision detonator based on HHT energy spectrum. *Explos. Shock Waves* **2017**, *37*, 107–113.
32. Forrest, J.; Hunt, H. A three-dimensional tunnel model for calculation of train-induced ground vibration. *J. Sound Vib.* **2006**, *294*, 678–705. [CrossRef]
33. Forrest, J.; Hunt, H. Ground vibration generated by trains in underground tunnels. *J. Sound Vib.* **2006**, *294*, 706–736. [CrossRef]
34. He, J.; Yu, Y.; Liang, W. Wavelet analysis for blasting seismic signals. *Chin. J. Geotech. Eng.* **1998**, *20*, 47–50.
35. Zhong, G.; Xiong, Z. Safety assessment of structure by blasting seism based on wavelet packet energy spectra. *Rock Soil Mech.* **2010**, *31*, 1522–1528.
36. Liu, J.; Wu, C.; Gao, Q. A research on predicting structural responses to blasting vibration. *Explos. Shock Waves* **2000**, *20*, 333–337.
37. GB 6722-2014. Safety Regulations for Blasting. Available online: https;//kns.cnki.net/kcms/detail/detail.aspx?dbcode=SCSF&dbname=SCSF00043577&uniplatform=NZKPT&v=OO0FuLDaHI7luGVfrOK6DjYozGQ1RhDsF2yc-9t9Ku-J7BLgdMhhtacmP-raAkL (accessed on 5 December 2014).
38. Li, X.; Ling, T.; Zhang, Y. *Analysis of Blast Vibration Signals-Theories and Methods*, 1st ed.; Science Press: Beijing, China, 2009; pp. 30–35.
39. Yu, J.; Liu, S.; Tong, L. Hollow effect induced by blasting vibration in shallow tunnels. *J. Southeast Univ. (Nat. Sci. Ed.)* **2010**, *40*, 176–179.
40. Shi, L.; Gao, W.; Wang, L. Experimental and numerical simulation study on blasting seismic effect of subway shallow buried tunnel. *Trans. Beijing Inst. Technol.* **2018**, *38*, 1237–1243.
41. Zhang, Z.; Zhou, C.; Lu, S.; Wu, C.; Zhang, C. Propagation characteristics of ground vibration induced by subsurface blasting excavation in an ultra-shallow buried underpass. *J. Cent. South Univ. (Sci. Technol.)* **2017**, *48*, 2119–2125.
42. Shen, J.; Yen, W.; O'Fallon, J. Interpretation and application of Hilbert-Huang transformation for seismic performance analysis. *Technol. Counc. Lifeline Earthq. Eng. Monogr.* **2003**, *25*, 657–666.